ANALYSIS OF BUOYANCY-DRIVEN VENTILATION OF HYDROGEN FROM BUILDINGS*

Barley, C.D.[1], Gawlik, K.[2], Ohi, J., and Hewett, R.
National Renewable Energy Laboratory,
1617 Cole Boulevard, Golden, Colorado 80401, USA
[1]dennis_barley@nrel.gov [2]keith_gawlik@nrel.gov

ABSTRACT

When hydrogen gas is used or stored within a building, as with a hydrogen-powered vehicle parked in a residential garage, any leakage of unignited H_2 will mix with indoor air and may form a flammable mixture. One approach to safety engineering relies on buoyancy-driven, passive ventilation of H_2 from the building through vents to the outside. To discover relationships between design variables, we combine two types of analysis: (1) a simplified, 1-D, steady-state analysis of buoyancy-driven ventilation and (2) CFD modeling, using FLUENT 6.3. The simplified model yields a closed-form expression relating the H_2 concentration to vent area, height, and discharge coefficient; leakage rate; and a stratification factor. The CFD modeling includes 3-D geometry; H_2 cloud formation; diffusion, momentum, convection, and thermal effects; and transient response. We modeled a typical residential two-car garage, with 5 kg of H_2 stored in a fuel tank; leakage rates of 5.9 to 82 L/min (tank discharge times of 12 hours to 1 week); a variety of vent sizes and heights; and both isothermal and non-isothermal conditions. This modeling indicates a range of the stratification factor needed to apply the simplified model for vent sizing, as well as a more complete understanding of the dynamics of H_2 movement within the building. A significant thermal effect occurs when outdoor temperature is higher than indoor temperature, so that thermocirculation opposes the buoyancy-driven ventilation of H_2. This circumstance leads to higher concentrations of H_2 in the building, relative to an isothermal case. In an unconditioned space, such as a residential garage, this effect depends on the thermal coupling of indoor air to outdoor air, the ground (under a concrete slab floor), and an adjacent conditioned space, in addition to temperatures. We use CFD modeling to explore the magnitude of this effect under rather extreme conditions.

NOMENCLATURE

c	=	Concentration of H_2, by volume (dimensionless, 0-1 in formulas, 0%-100% in graphs)
g	=	Acceleration of gravity = 9.81 m/s^2
h	=	Height between vents, m
A	=	Vent area (top = bottom), m^2
D	=	Vent discharge coefficient (dimensionless, 0-1)
D^*	=	Apparent value of D based on CFD results (dimensionless, 0-1)
F	=	Vent sizing factor (dimensionless)
NTP	=	Normal temperature and pressure (20°C and 1 atm)
P	=	Total pressure (Pa)
Q	=	Volumetric flow rate through a vent (m^3/s)
S	=	Source rate of H_2 (leak rate), m^3/s
Δ	=	Difference
δ	=	Ratio of densities of H_2/air at NTP = 0.0717 (dimensionless)
ρ	=	Density (kg/m^3)
φ	=	Stratification factor = c_T/c_{avg} (dimensionless)

Subscripts:

1,2,3,4	Locations shown in Fig. 1 (Section 2)
air	Properties of air
avg	Spatial average over the path 3-4 in Fig. 1 (Section 2)
o	Outdoor
B	Bottom vent
T	Top vent

1.0 INTRODUCTION

When hydrogen gas (H_2) is used or stored within a building, as with a hydrogen-powered vehicle parked in a residential garage or commercial service facility, any leakage of unignited H_2 will mix with indoor air and can potentially form a flammable mixture. The general approach to fire safety is to avoid a combination of fuel, an oxidizer, and heat (or spark) that completes the "fire triangle" and enables combustion. Oxygen is unavoidably present in occupied buildings. Also, the static electricity that is routinely generated by the movement of occupants is sufficient to ignite a mixture of H_2 and air [Ref. 1, p. 11]. Therefore, the only practical approach to safety in this context is to control the fuel so that a flammable mixture does not occur. The most widely accepted flammability range is 4.1% to 75% H_2 by volume [1]. To provide a safety margin, many standards [e.g. 2,3] specify a safe limit of 25% of the lower flammability limit (LFL), which for H_2 amounts to 1% by volume. Swain et al. [4,5] have measured the LFL in H_2 leakage jets between 6.6% and 8.1%. However, the current study involves H_2-air mixtures that are practically stationary, and we have no additional information regarding the relationship between velocity and LFL.

The well-known approaches to indoor air quality problems, of which this is an example, include (1) source control, (2) air treatment, (3) natural (passive) ventilation, and (4) mechanical ventilation. Source control involves preventing the infusion of a pollutant, H_2 in this case, into the indoor air. One method is to keep the fuel system outside the building. An automobile can be parked in a driveway or carport. Although this may be acceptable to some people, the use of residential garages is very well established and would be difficult to eliminate. Another source control method is quality control in the manufacture of vehicles, to limit the rate of fuel leakage, as in Standard SAE J2578 [6]. However, higher leakage rates must also be considered, as these may result from faulty repair work or collision damage after the car leaves the factory. Air treatment, or cleaning, involves the removal of a pollutant from indoor air. It may be possible to capture leaked H_2 within a building in a chemical process with either a mechanical or a passive apparatus. For example, H_2 does react with halogens. This is an area for possible future research. Concerns include reliability, response time, saturation capacity, reactant standby life, and cost.

In this paper we describe our analysis of buoyancy-driven, passive ventilation of H_2 from buildings through vents to the outside. Our goal is to ascertain the relationship between vent design, leakage rate, maximum concentration, and other variables, which leads to design guidelines, an understanding of the limitations of this approach, and recommendations for codes and standards. We pursue this goal by combining two types of analysis: (1) a simplified, one-dimensional, steady-state analysis of buoyancy-driven ventilation; and (2) computational fluid dynamics (CFD) modeling. The simplified model enables an algebraic solution that yields a closed-form expression relating the concentration of H_2 to vent size, height, and discharge coefficient; leakage rate; and a stratification factor. However, the stratification factor and vent discharge coefficient depend on dynamics that are beyond the scope of this model. The CFD modeling provides additional detail and indicates a range of the stratification factor needed to apply the simplified model. Because of the limitations of passive ventilation shown by this study, we also address mechanical ventilation rates.

The range and frequencies of occurrence of leakage rates that will occur with H_2 vehicles are unknown to us, despite our literature search. In an effort to bracket a range of possible leakage rates

and study sensitivities to this variable, we modeled rates ranging from 5.9 to 82 L/min, which correspond to leak-down times of 12 hours to 7 days for a 5-kg tank of H_2. We also calculate required mechanical ventilation rates over a wider range: 1.4 to 166 L/min, or 6 hours to 29 days. The 29-day leak-down time is based on a safety standard for vehicle manufacture [6]. We selected the 6-hour leakage rate arbitrarily, to provide an ample range for sensitivity study.

The TISEC *Sourcebook for Hydrogen Applications* [1] presents a compilation of basic information about H_2 properties, safety engineering, codes, and standards. Cadwallader and Herring [7] present similar general information as well as historical accounts of accidents involving H_2. Swain and Swain [8] have modeled transient accumulation rates of H_2 within a cloud above an H_2 leak in a passively ventilated room, with leak rates of 10 to 1000 L/min. Breitung et al. [9] have modeled transient H_2 cloud formation resulting from pulsed release of small amounts of H_2 (i.e., insufficient amounts to form a combustible concentration if fully mixed in the enclosure). Swain et al. have used helium to study H_2 leakage scenarios [10] and have tested H_2 ignition and combustion scenarios [4,5,11]. Papanikolaou and Venetsanos [12] have modeled three of the helium experiments performed by Swain et al. The present study addresses steady-state concentrations of H_2 resulting from sustained slow leaks; modeling of thermal effects due to high outdoor temperature; and passive vent sizing as a function of leakage rate and other variables.

2.0 SIMPLIFIED MODEL

The concept for the simplified model arose from the initial results of our CFD modeling, which is described in Section 3. Fig. 5 (Section 3) shows a typical steady-state H_2 stratification pattern computed by the CFD model. The concentration varies significantly in the vertical direction, but much less in the horizontal directions (except for the plume rising from the leak site). This suggests that a one-dimensional, steady-state analysis might capture the basic dynamics of this process and provide insights into relationships between variables. Indeed, the simplified model has proven useful in this manner. Previous researchers have conducted one-dimensional, steady-state analyses of thermally driven airflow through vents in vertical walls [13,14,15]. However, our literature search did not reveal any prior formulation relating gas concentration to leakage rate and vent size for ventilation driven by a buoyant gas.

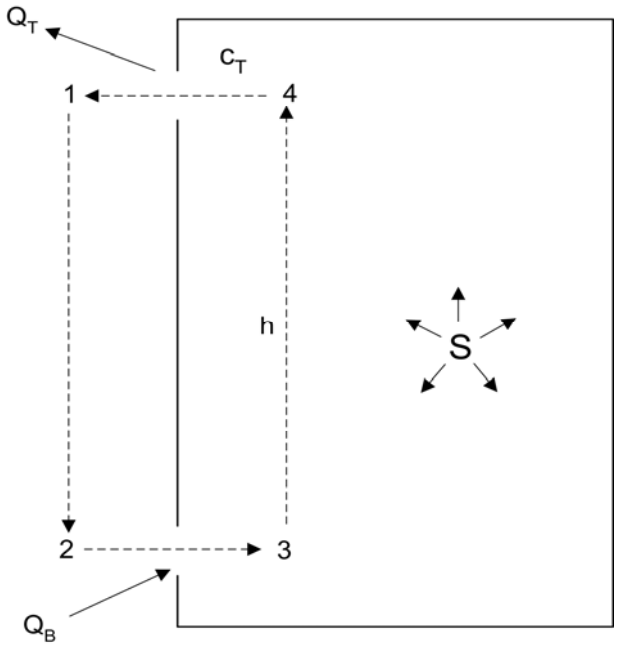

Figure 1. Illustration of the simplified model.

As shown in Fig. 1, we consider a source of H_2 gas (the leak) within an enclosure (such as a garage) with two vents to the outside, near the top and bottom of a side wall. To formulate the relationship between the buoyancy pressure and the pressure drops across the vents, we draw a closed contour (1-2-3-4) through both vents. Summing the total pressure differences around the loop, we write:

$$\Delta P_{1\text{-}2} + \Delta P_{2\text{-}3} + \Delta P_{3\text{-}4} + \Delta P_{4\text{-}1} = 0 \quad (1)$$

The two vertical segments of the loop (1-2 and 3-4) represent the buoyancy pressure as the difference between the weights of the inside and outside air columns. Assuming isothermal conditions between the garage interior and the outside air (thermal effects are discussed in Section 4):

$$\Delta P_{1\text{-}2} + \Delta P_{3\text{-}4} = g\, h\, \rho_{air}\, c_{avg}\, (1\text{-}\delta) \quad (2)$$

The relationship between pressure drop and airflow through the top vent is [16]:

$$Q_T = AD\sqrt{\frac{2\Delta P_{1-4}}{\rho_T}} \quad (3)$$

A similar equation applies to the bottom vent. The continuity equation for air and H_2 is:

$$Q_T = Q_B + S \quad (4)$$

The continuity equation for H_2 alone is:

$$Q_T\, c_T = S \quad (5)$$

Combining Eqns. 1 to 5 and reducing to a non-dimensional form results in this isothermal vent-sizing equation for buoyancy-driven ventilation:

$$F \equiv \frac{AD}{S}\sqrt{2gh} = \phi^{\frac{1}{2}}\left[\frac{1 - c_T(1-\delta) + (1-c_T)^2}{(1-\delta)\ c_T{}^3}\right]^{\frac{1}{2}} \quad (6)$$

The term involving the vent area, A, defined as the vent sizing factor, F, may also be thought of as the dimensionless vent area. It implies that the required vent area is proportional to the leakage rate and inversely proportional to the square root of the height between the vents, if other factors are constant. The right-hand term, involving the H_2 concentration, is more complex, because this factor enters the analysis in three places. The stratification factor, φ, occurs because the buoyancy force depends on the average H_2 concentration over the height (c_{avg} in Eqn. 2) whereas the continuity equation (Eqn. 5) involves the concentration at the top vent, c_T. (The density at the top vent also depends on c_T, in Eqn. 3.) It may seem counterintuitive that larger vents are required when the H_2 is more stratified. This relationship occurs because, given the same concentration at the top vent, there is less buoyancy in the indoor air column when the H_2 is less distributed over the height. The isothermal vent sizing equation (Eqn. 6), which is illustrated by the curves in Fig. 2, is useful for vent design purposes. However, values of the stratification factor, φ, and the vent discharge coefficient, D, are needed, and these are pursued in the following section.

3.0 CFD MODELING, ISOTHERMAL

CFD modeling provides detail and accuracy (pending experimental verification) beyond the capabilities of the simplified model and leads to a more thorough understanding of H_2 movement in the building. It includes 3-D geometry; diffusion, momentum, convection, and thermal effects; H_2

cloud tracking; and transient response. It can also indicate a range of the stratification factor needed to apply the simplified model for vent sizing.

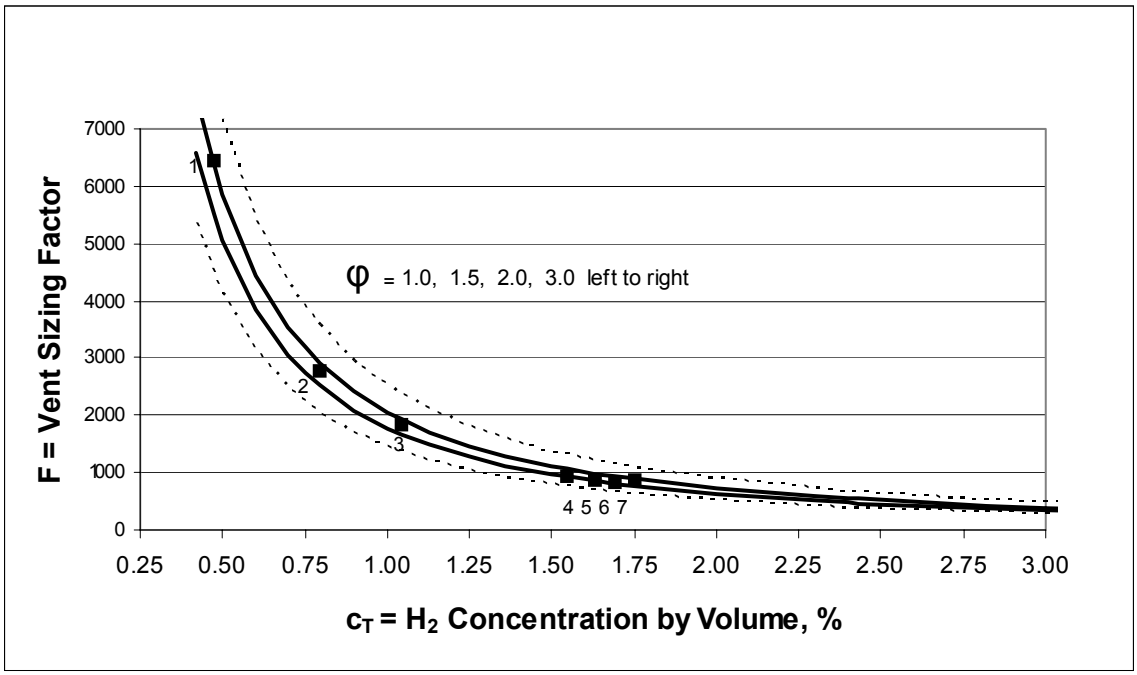

Figure 2. Comparison of simplified model (curves are based on Eqn. 6) and isothermal CFD results (points 1 to 7, Section 3)

.

Figure 3. Home used for isothermal CFD case study (Cases 1-7), built by Pulte Homes in Las Vegas, Nevada. Courtesy of the Building America Program [17].

For our initial case study we selected a typical home, shown in Fig. 3, which features a two-car garage with an A-frame roof. The garage floor is 6.40 m wide by 6.71 m deep. The roof slope is 5/12, and the roof ridge is 4.06 m above the floor. The garage volume is 146 m^3. In this case study we assume the garage is an isolated zone with no transfer of H_2 into the remainder of the house. The assumed leak source is a vehicle fuel tank containing 5 kg of pressurized H_2 gas. This amount of H_2 occupies a volume of 59.7 m^3 at NTP, which amounts to 41% of the garage volume; so a uniform mixture of 10

times the LFL is possible. Tank pressures of 340 to 680 atm (34.5 to 68.9 MPa) are to be expected, although the pressure does not enter our computations directly. We modeled leakage rates ranging from 5.9 to 83 L/min, corresponding to tank leak-down times of 12 hours to 1 week. To reduce the required computational effort, we set up our model with bilateral symmetry, so we model half of the garage and the results represent each half. The leak is located 1.07 m above the floor, approximating the height of a leak from a vehicle, under the roof ridge, halfway between the front and back of the garage. The rectangular vents are located in the front wall, under the roof ridge, one adjacent to the floor (in the garage door) and the other as near to the roof ridge as we can locate it in the triangular gable.

We used the FLUENT version 6.3.26 CFD software [18]. We used the poly mesh option for computational economy, with first order discretization of convection and time for speed and stability. A sensitivity study showed that the solution is insensitive to grid density at about 40,000 cells. Evidently, this grid density is sufficient to minimize the effects of numerical diffusion.[1] We then used this grid density for our further computations. The average size of a grid cell is about 1.8 L, although we used a higher mesh density near the leak and the vents where gradients are high. We used both the renormalization group (RNG) k-ε turbulence model with the differential viscosity option enabled and the laminar model. The results indicate turbulence intensities lower than 1% in more than 85% of the domain in all the cases we ran, and more than 90% of the domain in four of the cases. Other researchers have found that k-ε turbulence models tend to overpredict mixing of gas released from slow leaks [12], thus underpredicting stratification, and the use of a laminar model will lead to a more stratified hydrogen distribution [9]. Based on Eqn. 6 and Fig. 2, higher stratification corresponds to higher H_2 concentrations for a given vent size. Thus, the laminar model is more conservative for our purpose of safety engineering, so we proceeded to use the laminar model for the results we are reporting here. We modeled the inlet and outlet vents as pressure boundary conditions. The model determines static pressure differences due to hydrostatic head outside of the inlet and outlet vents, based on the specified ambient outdoor air density corresponding to the simulation conditions. The incompressible ideal gas law is used to determine indoor density as a function of temperature and the air-hydrogen mixture. Because the boundary of our grid corresponds to the garage envelope, we found it necessary to disable diffusion across the boundary in order to eliminate spurious H_2 diffusion across the abrupt concentration gradient at the outlet vent, which would not occur in reality. Time steps were changed during the course of the simulation to speed convergence. Initially, the time step was 0.1 seconds to capture the transient behavior as the leak started. When the iterations to convergence at each time step dropped to below 10, the time step was doubled. The largest time step used was 0.4 seconds. Data and image files were saved every 10 minutes of flow time.

An actual leak from a pressurized tank might occur at a high velocity in any direction. On the other hand, if a leak occurs within the body of the car, H_2 may emanate from the car at a low speed. We modeled the source of the leak as an 8-cm sphere from which H_2 emanates at the lowest possible speed, driven only by displacement. We believe this is a worst-case scenario, because our modeling has shown that (1) momentum effects tend to augment buoyancy in driving vent flow and lead to lower H_2 concentrations, and (2) momentum tends to destratify the H_2-air mixture, which also leads to lower concentrations (see Eqn. 6 and Fig. 2). More modeling is needed to determine more specifically the effects of leakage velocity. In addition to plotting the concentration throughout the garage periodically, we also monitored the concentration at the outlet vent to determine when steady-state conditions were established. The modeling described in this section does not include thermal effects, which are described in Section 4.

[1] Numerical diffusion is a consequence of discretizing into finite-difference equations the continuous Navier-Stokes equations of fluid motion. The discretized equations tend to exhibit greater diffusion than the continuous equations. One method to minimize numerical diffusion is to increase grid density until the converged solution does not change. Another method is to use higher order discretization schemes, but they can introduce instability in the solution process.

In order to compare results of our CFD model with the simplified model, we ran the series of cases listed in Table 1 and plotted as points 1 to 7 in Fig. 2. In each case, the computation was continued until a steady-state condition was observed. Fig. 4 ("No Thermal Effects" curve) shows a typical transient response of the concentration at the top vent, although the time to steady state and the final concentration vary from case to case. Fig. 5 shows a typical stratification pattern under steady-state conditions, and Fig. 6 shows corresponding vertical concentration profiles at four locations in the garage.

Table 1. Series of CFD cases plotted in Fig. 2.

Specifications, Results	CFD Case						
	1	2	3	4	5	6	7
Leak-Down Time, hr/5 kg	168	72	48	24	24	24	12
Vent Size, cm^2	788	788	788	788	788	788	1576
Vent Offset, cm	0.0	0.0	0.0	0.0	15.2	30.5	0.0
Vent Height, m	3.650	3.650	3.650	3.650	3.345	3.040	3.599
H_2 Conc. at top vent, % Vol.	0.47	0.79	1.04	1.55	1.63	1.69	1.75
Straification Factor (φ)	1.65	1.67	1.67	1.52	1.58	1.59	1.88
Discharge Coeff. (D*)	0.952	0.952	0.952	0.965	0.948	0.944	0.903

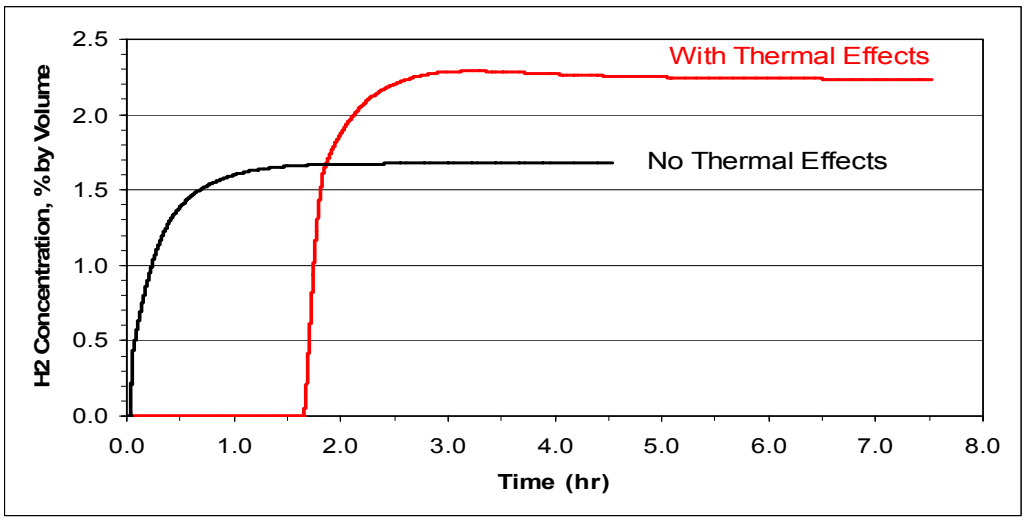

Figure 4. Development of H_2 concentration at the top vent for Case 8, showing the trend to steady state.

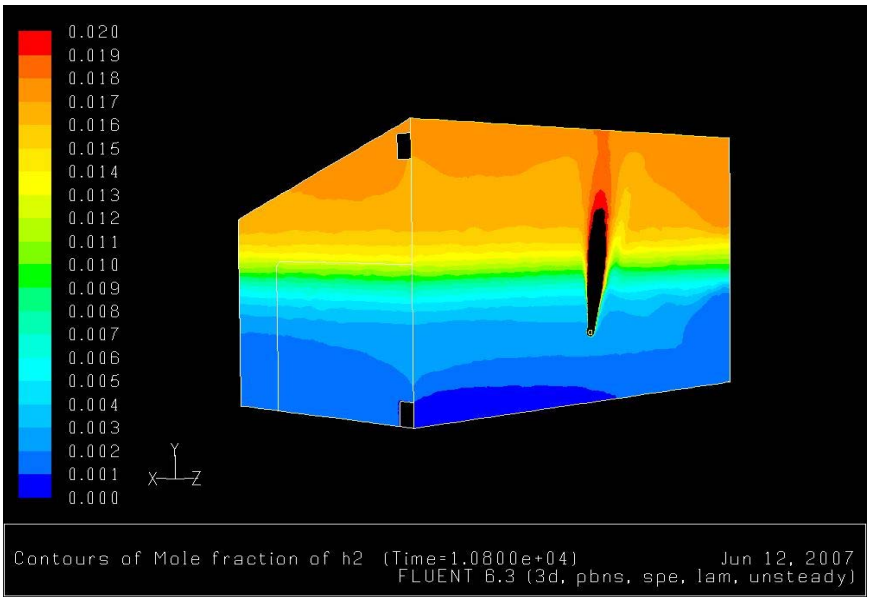

Figure 5. Graphic result of CFD modeling for Case 7. Left half of garage in Fig. 3 is shown here. Color scale is H_2 mole fraction; the full-scale value of 0.02 is equivalent to 2% H_2 by volume. Elapsed time is 3 hours (steady state).

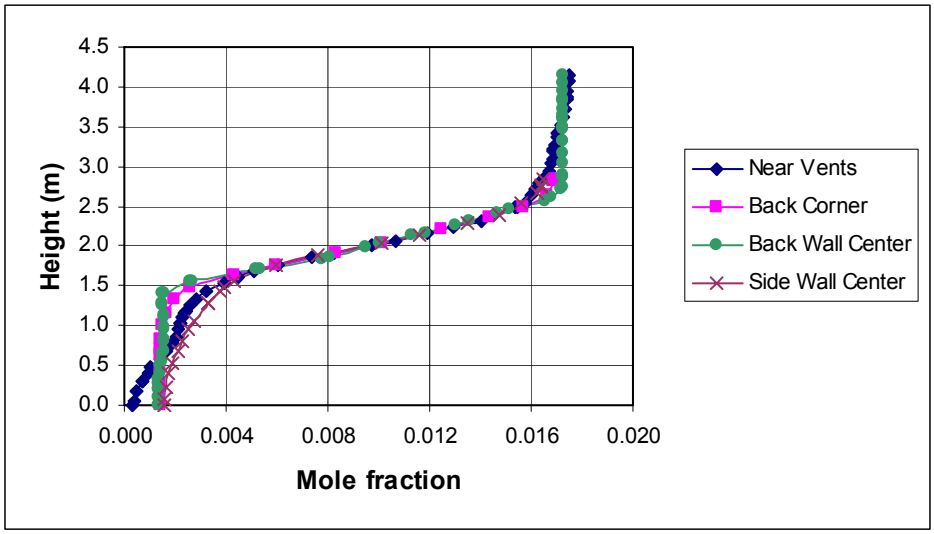

Figure 6. Vertical H_2 concentration profiles at 4 locations in garage, corresponding to Fig. 5 and Case 7.

We modeled the vents as open rectangles with no thickness and an aspect ratio of 4:3. As part of the comparison between the simplified model and the CFD results, we calculated values of the apparent vent discharge coefficient based on the density of the H_2-air mixture and flow rates through the vents indicated by the CFD model. From Eqns. 1 and 3,

$$D = \left[\frac{\rho_T Q_T^{\,2} + \rho_o Q_B^{\,2}}{2A^2 gh(\rho_o - \rho_{avg})} \right]^{\frac{1}{2}} \tag{7}$$

This formulation assumes equal values of D for the top and bottom vents, and it assumes that the flow through the vents is driven only by the static pressure difference. However, airflow in the CFD model may also be driven by momentum generated in the buoyant rise of H_2 from the leak site. We use the symbol D^* to denote the apparent value of D given by Eqn. 7 with Q_T, Q_B, ρ_T, and ρ_{avg} as computed by the CFD model. Values of D^* determined by this method range from 0.903 to 0.965 (Table 1). This range is significantly higher than published values of D for similar configurations. Resistance coefficients reported by Idelchik [19] for orifices in a thin wall with infinite surface area correspond to a value of about D = 0.60. Building Science Consulting [20] cites a value of D = 0.61 for sizing transfer grilles for return air flows in residential forced-air systems. American Lung Association guidelines for sizing transfer grilles correspond to D = 0.72 [21]. Possible reasons for the difference between the published values of D and our values of D^* include (1) the significance of momentum effects in driving airflow through the vents; (2) differences in the flow regime, indicated by the Reynolds number,[2] between our scenario and the literature references; (3) differences in geometry; and (4) CFD modeling issues. Further study, including model validation, is needed to understand this result. In the meantime, based on the literature references, the value D = 0.60 seems to be a reasonably conservative value for design purposes. In Cases 5 and 6, compared to Case 4, we explored the effect of offsetting the bottom vent above the floor and the top vent further from the roof ridge. The value of D^* decreases slightly with increasing offset (Table 1), although the effect does not appear to be very significant.

Values of the stratification factor, φ, range from 1.52 to 1.88 (Table 1). The agreement between the simplified model and the CFD results is indicated in Fig. 2 by points 1 to 7 lying between the solid curves for φ = 1.5 and 2.0. However, some differences between the two models (such as momentum effects) are absorbed in the values of D^* that were calculated as described above and used in plotting points 1 to 7. Based on these results, the value φ = 2.0 appears to be reasonably conservative, pending model validation and further case studies.

4.0 CFD MODELING, THERMAL EFFECTS

Both the simplified model described in Section 2 and the CFD modeling described in Section 3 are based on assumed isothermal conditions. In this section we consider two thermal effects that may influence passive ventilation of H_2.

4.1 Expansion Heating

Ordinarily, when many real gases expand from a higher to a lower pressure at normal temperatures (e.g. 293 K), their temperatures decrease, such as when air is vented from an automobile tire. However, because the Joule-Thomson inversion temperature for H_2 is 202 K [22], the temperature of H_2 may increase upon expansion, depending on the leak velocity. A maximum possible temperature rise of 30.1 K would occur if the leak occurred in both an adiabatic and an isenthalpic manner, as we have modeled it. Although this leakage scenario is not realistic, it does indicate the limiting case of maximal expansion heating. Based on the ideal gas law, this absolute temperature rise of about 10% corresponds to a density decrease of about 10%. However, based on the difference between the densities of air and H_2, the buoyancy force is affected by less than 1%. This rules out any significant benefit of additional buoyancy due to expansion heating. In our modeling of the garage shown in Fig.

[2] For cases 1-7, the Reynolds number (Re) for airflow through the top vent ranges from 4,700 to 9,100. The Idelchik reference is based on Re ≥ 10,000. The other literature references do not cite values of Re.

3, the effect of including expansion heating in our model is negligible compared to the other effects we are studying.

4.2 Reverse Thermocirculation

A more significant thermal effect occurs when the outdoor air temperature is higher than the garage air temperature. Thermocirculation (the stack effect) opposes the buoyancy-driven ventilation of H_2, and warmer outside air may enter the top vent while H_2 accumulates near the ceiling. At the same time, the garage temperature is affected by the inflow of outside air as well as the thermal coupling between the garage and (1) the conditioned space in the home, and (2) the ground temperature, as through a concrete slab floor, and (3) the outdoor air by conduction through the envelope surfaces. Transient effects related to the thermal mass of the garage may also affect the garage temperature, although we did not model these effects. Such an outdoor-indoor temperature difference may occur on a hot day, with a garage that has strong thermal coupling to a low ground temperature and an air-conditioned space and a low thermal coupling to the ambient air by conduction. Alternatively, a large temperature difference may occur on a cold morning, if the ambient air warms faster than a cold garage with significant thermal mass. The resulting H_2 concentration can be significantly higher than that predicted by the isothermal models.

In order to study the potential magnitude of this effect, we modeled a rather extreme hot-day scenario. We selected a home, shown in Fig. 7, with strong thermal coupling from the garage to the conditioned space (80.3 W/°C) and to the ground (32.7 W/°C) and weak thermal coupling to the outside air by conduction (16.4 W/°C). We assumed a high outdoor temperature (40.6°C), a low ground temperature (10°C), and a low air-conditioning setpoint (21.1°C). This garage is 6.40 m wide, 7.24 m deep, and 2.59 m high. We modeled the ambient temperature as a constant to explore steady-state effects. However, in reality, the ambient temperature varies with time, and thermal mass effects, which we did not model, are important. We modeled three cases with significantly different results.

In Case 8 we used the 24-hour leak rate with 0.121 m^2 vents based on the isothermal vent sizing equation with $c_T = 2\%$, $\varphi = 2.0$ (so F = 723), and D = 0.60. As shown in Fig. 8, outside air initially flows in the top vent, causing H_2 to accumulate in the top rear area of the garage. After about 1.7 hours, the H_2 buoyancy overcomes the reverse thermocirculation and begins escaping through the top vent. Fig. 4 shows the transient H_2 concentration at the top vent compared to the same case with thermal effects disabled. The thermal case exceeds the design limit of 2% H_2, (maximum 2.3%) whereas the isothermal case does not. The steady-state, volume-average garage air temperature is 37.8°C in this case.

Figure 7. Home used for CFD thermal case study (Cases 8 to 10), built by Heartland Homes in Pittsburgh, Pennsylvania. Courtesy of the Building America Program [17].

In Case 9 we used the 7-day leak rate with 494 cm^2 vents based on the isothermal vent sizing equation with c_T = 1%, φ = 2.0 (so F = 2061), and D = 0.60. Because of the smaller vents, the garage remains cooler in this case than in Case 8 (36.4°C in the steady state). Also, because of the lower leak rate, the H_2 destratifies more before reaching a high concentration. In the steady-state condition shown in Fig. 9, H_2 is escaping through the *bottom* vent while reverse thermocirculation continues. The maximum H_2 concentration in the garage, away from the plume, is about 1%, which is the same as the isothermal design value, although this agreement is considered coincidental.

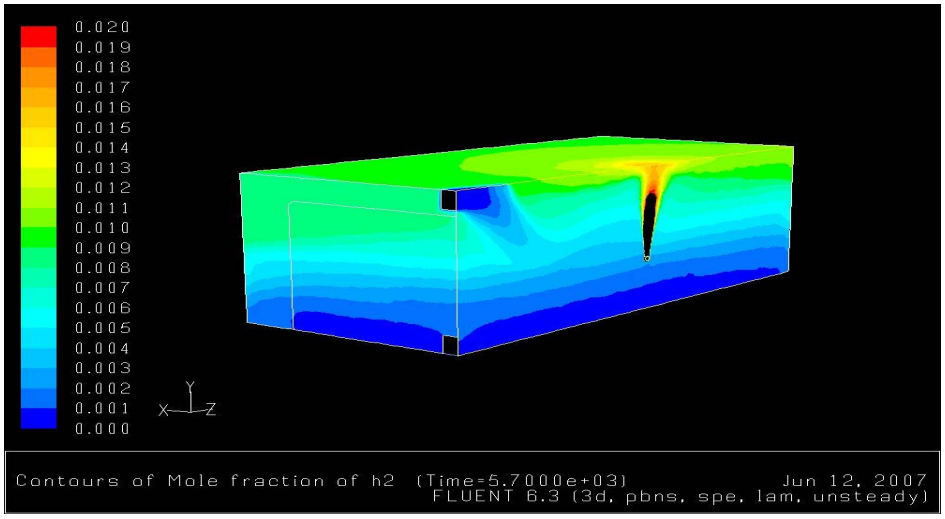

Figure 8. Graphic result of CFD modeling for thermal Case 8. Left half of garage in Fig. 7 is shown here. Color scale is H_2 mole fraction; the full-scale value of 0.02 is equivalent to 2% H_2 by volume. Elapsed time is 1.6 hours (transient response).

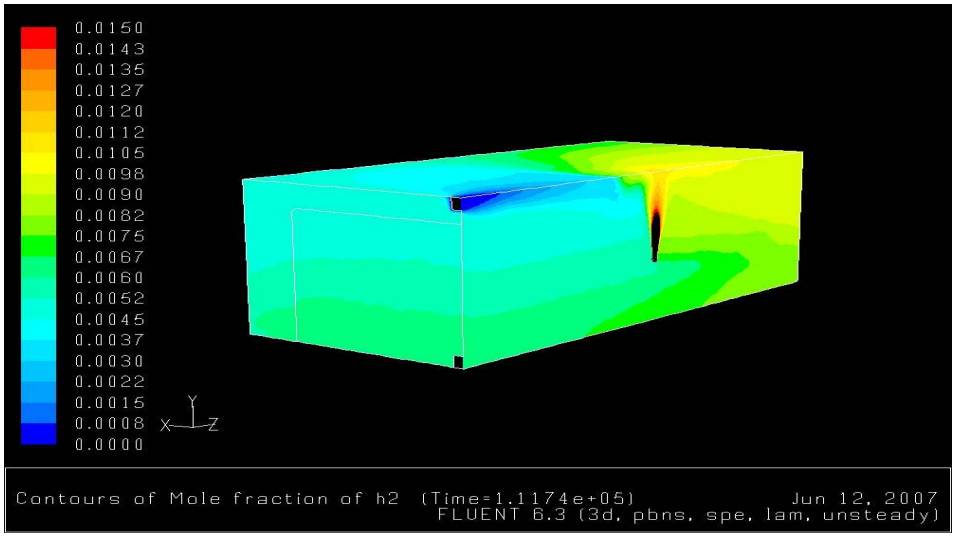

Figure 9. Graphic result of CFD modeling for thermal Case 9. Left half of garage in Fig. 7 is shown here. Color scale is H_2 mole fraction; the full-scale value of 0.015 is equivalent to 1.5% H_2 by volume. Elapsed time is 31 hours (steady state).

In an effort to identify a "perfect storm" scenario, we modeled an additional leakage rate between the previous two cases with opposite vent flow directions in the steady state. In Case 10 we used the 3-day leak rate with 405 cm^2 vents based on the isothermal vent sizing equation with c_T = 2%, φ = 2.0

(so F = 723), and D = 0.60. In the steady state, H_2 escapes through the top vent, with a maximum concentration of 5% away from the plume. This is the most significant thermal effect in the cases we have studied to date, with the H_2 concentration reaching 2.5 times the value predicted by the isothermal vent sizing equation. However, this is not necessarily the worst-case scenario.

Based on Cases 8 to 10, high outdoor temperature may or may not increase the H_2 concentration relative to an isothermal case. As a safety engineering concern, this is a risk factor. Further study is needed to ascertain the maximum increase in H_2 concentration that may result from reverse thermocirculation.

5.0 WIND EFFECTS

Wind pressure on a building may affect the buoyancy-driven ventilation of H_2. Depending on the direction of the wind relative to the locations of the inlet and outlet vents, the wind may either help or hinder the ventilation. Under some conditions, a vent design that would otherwise limit the H_2 concentration to the safe limit might be rendered ineffective because of wind effects. These effects are difficult to model and describe parametrically because of the sensitivity of the wind pressure at the vent locations to wind speed and direction, surrounding terrain and buildings, and fine details of the building architecture. Thus, we have not included wind effects in our analysis. One approach to minimizing the likelihood of adverse wind effects would be to locate the inlet (bottom) vent on the prevailing upwind side of the building and the outlet (top) vent on the prevailing downwind side. In this configuration, the prevailing winds would most likely augment, rather than opposing, the buoyancy-driven ventilation of H_2 from the building.

6.0 MECHANICAL VENTILATION

Because buoyancy-driven passive ventilation has limitations, we also consider the alternative approach of mechanical ventilation. With reference to Fig. 1 and Eqn. 5, we calculate the required airflow rate, Q_T, through an exhaust fan placed in the top vent as a function of the leakage rate, S, and the concentration at the outlet, c_T. IEC Standard 60079-10 [23] presents a similar formulation, which also accounts for airflow impediments and a temperature correction, with the result expressed in terms of an effective cloud volume based on the actual net ventilation rate. With our formulation, applying the safe limit value of c_T = 1%, the indicated airflow rates are shown in Table 2. For perspective, we note that airflow rates for bathroom exhaust fans and whole-house ventilation systems are typically in the range of about 25 to 50 L/s. For leak-down times of 1 day and less, the ventilation rates listed in Table 2 are significantly higher than this range. Constant operation of such a fan does not seem practical, because of both the fan energy consumption and the effect on garage temperature in cold weather. Thus, a fan controller based on H_2 detection would be recommended, and the reliability of the control system would be essential to safety.

Table 2. Fan sizing chart for mechanical ventilation, based on c_T = 1%.

Leakage Rate (Based on 5 kg of H_2)			Fan Airflow
T, days	T, hrs	L/min	L/s
0.25	6	166	276
0.5	12	82.9	138
1	24	41.5	69
2	48	20.7	35
3	72	13.8	23
7	168	5.92	9.9
29	696	1.43	2.4

7.0 CONCLUSIONS

A significant uncertainty in this analysis is the range of leakage rates that will occur with H_2 vehicles. We have modeled and tabulated results for a range of leakage rates in order to indicate sensitivities to this variable. Further research is needed to ascertain the occurrence probabilities of various leakage rates.

Our CFD model has not yet been compared with experimental results as a check on its accuracy. Our research plan includes this work as a future activity.

The reverse thermocirculation effect can occur in nearly any climate because of steady-state or transient temperature differences between the garage and the ambient air. These effects can inhibit buoyancy-driven ventilation to the extent that H_2 concentrations will exceed values predicted by the isothermal models. In a "perfect storm" scenario we crafted with respect to architecture, weather, and leak rate (Case 10), the thermal effect increased the expected H_2 concentration from 2% to 5%. This is a significant risk factor, although the likelihood if its occurrence may be low, judging by the lengths we went to in order to identify a significant example.

Based on our results to date, a reasonably conservative approach to sizing vents for passive ventilation of H_2 is to use the isothermal vent sizing equation (Eqn. 6) with the values $c_T = 0.01$, $\varphi = 2$, and $D = 0.6$. However, the value $\varphi = 2$ is subject to CFD model validation and further case studies. Also, wind effects and outdoor temperatures higher than the garage temperature are additional risk factors, along with uncertainty about leakage rates

Mechanical ventilation is an alternative approach to safety. Because of the large airflow rates indicated by Table 2, an H_2-sensing fan controller is recommended. Research is needed to develop a control system that is sufficiently reliable and economical for residential use.

8.0 ACKNOWLEDGMENTS

This work is funded by the Hydrogen Safety, Codes and Standards program of the U.S. Department of Energy's Office of Hydrogen, Fuels Cells and Infrastructure Technologies at the Hydrogen Technologies and Systems Center of the National Renewable Energy Laboratory (NREL), in collaboration with NREL's Buildings and Thermal Systems Center.

9.0 REFERENCES

1. Bain, A., Barclay, J.A., Bose, T.K., Edeskuty, F.J., Fairlie, M.J., Hansel, J.G., Hay, D.R., Swain, M.R., Ohi, J.M. and Gregoire Padró, C.E. Sourcebook for Hydrogen Applications, 1998, TISEC, Inc., Montreal, Canada.
2. ICC. *International Fire Code*, Section 2211.7.1.1, 2006, International Code Council, Washington, DC. http://www.iccsafe.org, last accessed 6/5/07.
3. NFPA. Vehicular Fuel Systems Code, Section 9.3.3.5.4.1, 2006, National Fire Protection Association, Quincy, MA. http://www.nfpa.org/, last accessed 6/12/07.
4. Swain, M.R., Filoso, P.A. and Swain, M.N. Ignition of Lean Hydrogen-Air Mixtures, *Int. J. Hydrogen Energy*, 30, No. 30, 2005, pp. 1447-1455.
5. Swain, M.R., Filoso, P.A. and Swain, M.N. An Experimental Investigation into the Ignition of Leaking Hydrogen, *Int. J. Hydrogen Energy,* 32, No. 2, 2007, pp. 287-295.
6. Standard SAE J2578. Surface Vehicle Recommended Practice, 2002, SAE International, Warrendale, PA. http://www.sae.org/servlets/index, last accessed 4/27/07.

7. Cadwallader, L.C. and Herring, J.S. Safety Issues with Hydrogen as a Vehicle Fuel, Idaho National Engineering and Environmental Laboratory, Lockheed Martin Idaho Technologies Company, Report No. INEEL/EXT-99-00522.
8. Swain, M.R. and Swain, M.N. Passive Ventilation Systems for the Save Use of Hydrogen, *Int. J. Hydrogen Energy*, 21, No. 10, 1996, pp. 823-835.
9. Breitung, W., Necker, G., Kaup, B. and Veser, A. Numerical Simulation of Hydrogen Release in a Private Garage, Proceedings of Hypothesis IV, 9-14 September 2001, Strahlsund, Germany, p. 368.
10. Swain, M.R., Filoso, P., Grilliot, E.S. and Swain, M.N. Hydrogen Leakage into Simple Geometric Enclosures, *Int. J. Hydrogen Energy*, 28, No. 2, 2003, pp. 229-248.
11. Swain, M.R. Fuel Leak Simulation. Proceedings of the 2001 U.S. DOE Hydrogen Program Review, 17-19 April 2001, Baltimore, MD, pp. 679-689, NREL Report No. CP-610-30535, http://www.nrel.gov/docs/fy01osti/30535.pdf.
12. Papanikolaou, E.A. and Venetsanos, A.G. CFD Modeling for Helium Releases in a Private Garage without Forced Ventilation, Proceedings of the Fist ICHS, Pisa, Italy, 8-10 September 2005, http://conference.ing.unipi.it/ichs2005/index.html, last accessed 4/27/07.
13. Emswiler, J.E. The Neutral Zone in Ventilation. *Trans. Amer. Soc. Heat. Vent. Engrs.*, 32, 1926, pp. 59-74.
14. Brown, W.G. and Solvason, K.R. Natural Convection through Rectangular Openings in Partitions—1. *Int. J. Heat Mass Transfer*, Vol. 5, 1962, pp. 859-868.
15. Fitzgerald, S.D. and Woods, A.W. Natural Ventilation of a Room with Vents at Multiple Levels. *Building and Environment*, Vol. 39, 2004, pp. 505-521.
16. ASHRAE. *Handbook—Fundamentals*, Chapter 27, Eqn. 28. American Society of Heating, Refrigerating, and Air-Conditioning Engineers, Inc., 2005, Atlanta, GA.
17. Building America homepage, http://www.eere.energy.gov/buildings/ building_america/, last accessed 4/26/07.
18. Fluent, Inc., Lebanon, NH, http://www.fluent.com/, last accessed 4/26/07.
19. Idelchik, I.E. *Handbook of Hydraulic Resistance*, 2nd Ed, Diagram 4-18. Hemisphere Publishing Corp., 1986, New York, NY.
20. Building Science Consulting. Discussion of the Use of Transfer Grilles to Facilitate Return Air Flow in Central Return Systems, http://www.buildingscienceconsulting.com/resources/mechanical/ hvac/transfer_grills.htm, last accessed 4/26/07.
21. American Lung Association. American Lung Association Health House Builder Guidelines, Effective 10/1/04, The American Lung Association, 2004, New York, NY.
22. Lindeburg, M. *Mechanical Engineering Review Manual*, 7th ed., Professional Publications, Inc., 1984, Belmont, CA, pp. 6-21.
23. IEC. International Standard 60079-10: *Electrical apparatus for explosive gas atmospheres*, Annex B, Sec. B.4.2.2, 2002, International Electrotechnical Commission, Geneva, Switzerland. http://www.iec.ch/, last accessed 6/19/07.